Since January 2020 Elsevier has created a COVID-19 resource centre with free information in English and Mandarin on the novel coronavirus COVID-19. The COVID-19 resource centre is hosted on Elsevier Connect, the company's public news and information website.

Biomedicine & Pharmacotherapy 150 (2022) 113021

Contents lists available at ScienceDirect

Biomedicine & Pharmacotherapy

journal homepage: www.elsevier.com/locate/biopha

Ursodeoxycholic acid ameliorates cell migration retarded by the SARS-CoV-2 spike protein in BEAS-2B human bronchial epithelial cells☆

Pham Xuan Thuy, Tran Duc Duy Bao, Eun-Yi Moon *

Department of Integrated Bioscience and Biotechnology, Seoul 05006, Republic of Korea

ARTICLE INFO

Keywords:
Ursodeoxycholic acid (UDCA)
SARS-CoV-2 spike protein
ACE2
Beas-2B bronchial epithelial cell
Cell migration

ABSTRACT

Background: Coronavirus disease 2019 (COVID-19) is caused by severe acute –respiratory syndrome coronavirus 2 (SARS- CoV-2) through interaction of the spike protein (SP) with the receptor-binding domain (RBD) and its receptor, angiotensin converting enzyme 2(ACE2). Repair mechanisms induced following virus infection can restore the protective barrier through wound healing. Then, cells from the epithelial basal layer repopulate the damaged area, followed by cell proliferation and differentiation, as well as changes in gene expression.
Methods: Using Beas-2B cells and SP, we investigated whether ursodeoxycholic acid (UDCA) contributes to restoration of the bronchial epithelial layer. ACE2 expression was measured by RT-PCR and Western blotting. SP–ACE2 interaction was analyzed by flow cytometry and visualized through immunostaining. Cell migration was assessed using single cell path tracking and wound healing assay.
Results: Upon ACE2 overexpression in HeLa, HEK293T, and Beas-2B cells following the transfection of pCMV-ACE2 plasmid DNA, SP binding on each cell was increased in the ACE2 overexpression group compared to pCMV-transfected control cells. SP treatment delayed the migration of BEAS-2B cells compared to the control. SP also reduced cell migration, even under ACE2 overexpression; SP binding was greater in ACE2-overexpressed cells than control cells. UDCA interfered significantly with the binding of SP to ACE2 under our experimental conditions. UDCA also restored the inhibitory migration of Beas-2B cells induced by SP treatment.
Conclsion: Our data demonstrate that UDCA can contribute to the inhibition of abnormal airway epithelial cell migration. These results suggest that UDCA can enhance the repair mechanism, to prevent damage caused by SP–ACE2 interaction and enhance restoration of the epithelial basal layer.

1. Introduction

Coronavirus disease 2019 (COVID-19) is caused by severe acute respiratory syndrome coronavirus 2 (SARS-CoV-2), [1] which was first reported in Wuhan, China [2,3]. COVID-19 spread worldwide, emerging as a global pandemic [4]. SARS-CoV-2 uses the SARS-CoV receptor angiotensin converting enzyme 2 (ACE2) for entry [5,6], and the serine protease TMPRSS2 for spike protein (SP) priming [5]. Electron microscopy shows that ACE2 receptor decorates the knobs at the wider end of SP trimers [6]. SP is a large type I transmembrane protein containing two subunits, S1 and S2. S1 consists mainly of a receptor-binding domain (RBD) that is responsible for recognizing the cell surface ACE2 receptor, whereas S2 contains basic elements needed for membrane fusion [7]. The interaction of SARS-CoV-2 SP and ACE2 has been found to be a major determinant of virus replication and disease severity [5,8].

Airway epithelial cells play a role in the protection of airway mucosa from various sources of injury, including viruses. Structural and functional alteration of these cells allows them to rapidly adapt to local environmental changes or repair the epithelium following injury [9–11]. Airway epithelial cell migration plays a pivotal role in airway repair [12]. The migration of neighboring cells is an important component in the rapid repair of damaged airway epithelia [13]. Therefore, it is

Abbreviations: ACE2, angiotensin converting enzyme 2; DAPI, 6-diamidino-2-phenylindole; MTT, [3(4,5-dimethyl-thiazol-2-yl)– 2,5-diphenyl tetrazolium bromide]; RBD, receptor binding domain; SARS- CoV-2, severe acute respiratory syndrome coronavirus; SP, spike protein; UDCA, ursodeoxycholic acid.

☆ The English in this document has been checked by at least two professional editors, both native speakers of English. For a certificate, please see: http://www.textcheck.com/certificate/13YaMR.

* Correspondence to: Department of Integrated Bioscience and Biotechnology, Sejong University, 209 Neungdong-ro Kunja-Dong Kwangjin-Gu, Seoul 05006, Republic of Korea.

E-mail address: eunyimoon@sejong.ac.kr (E.-Y. Moon).

https://doi.org/10.1016/j.biopha.2022.113021
Received 4 March 2022; Received in revised form 7 April 2022; Accepted 20 April 2022
Available online 25 April 2022

important to determine whether SARS-CoV-2 impairs airway epithelial cell migration, and molecules that may stimulate the regeneration of functional airway epithelia after loss of cellular epithelial integrity due to SARS-CoV-2 are of particular interest.

Ursodeoxycholic acid (3α, 7β-dihydroxy-5β-cholanic acid, UDCA) is a hydrophilic dihydroxy bile acid that is commercially available for the remediation of various hepato-cholestatic disorders [14]. UDCA has been found to have non-hepatic effects in various pathophysiological models, such as cystic fibrosis lung disease [15], airway inflammation [16,17], colorectal carcinoma [18], and Parkinsonism [19]. UDCA also interacts in two distinct regions of SP sequences. UDCA may remain bound to the membrane, inhibiting the entry of SARS-CoV-2 into the host cell [20] through reduced RBD–ACE2 binding [21]. However, the physiological effects of UDCA on airway epithelium regeneration remain poorly understood.

In this study, we used Beas-2B human bronchial epithelial cells to investigate the potential role of UDCA in the airway epithelium regeneration following damage caused by SARS-CoV-2 SP.

2. Materials and methods

2.1. Reagents

Ursodeoxycholic acid (UDCA, 15121) was purchased from Cayman Chemical (Ann Arbor, MI, USA). MTT [3(4,5-dimethyl-thiazol-2-yl)-2,5-diphenyl tetrazolium bromide] (M5655), DAPI (D9542) and bovine serum albumin (BSA, A3059) were purchased from Sigma Chemical Co. (St. Louis, MO, USA). CellTiter-Glo® Luminescent cell viability assay kit (G9241) was purchased from Promega Co. (Madison, WI, USA). Mouse antibodies which are reactive with acetylated tubulin (T7451) were from Sigma-Aldrich Co. (St. Louis, MO, USA). Polyethylenimine (PEI, 02371) was purchased from Polysciences, Inc. (Warrington, PA, USA). Rabbit antibodies which are reactive with Flag (14793) were from Cell Signaling Technology Inc. (Danvers, MA, USA). FITC-conjugated streptavidin (554061) and PE-conjugated streptavidin (554060) were purchased from BD Bioscience (Franklin Lakes, NJ, USA). Flag-tagged human pCMV-ACE2 plasmid (HG10108-CF) and a biotinylated SARS-CoV-2 (2019-nCoV) spike protein, RBD (40592-V08B-B) were purchased from Sino Biological Inc. (Wayne, PA, USA). Fibronectin (5050) and bovine collagen type I (5005) were purchased from Advanced BioMatrix, Carlsbad, C, USA). Except where indicated, all other materials are obtained from the Sigma Chemical Co. (St. Louis, MO, USA).

2.2. Cell culture

Beas-2B human bronchial epithelial cells (ATCC # CRL-9609) were obtained from Korea research institute of bioscience and biotechnology (KRIBB) cell bank (Daejeon, Rep.of Korea). Beas-2B cells are isolated from normal bronchial epithelium of noncancerous individuals. The cells are able to undergo squamous differentiation in response to serum. Cells were cultured as monolayers in Dullecco's modified Eagle's medium (DMEM) with supplement of 10% fetal bovine serum (FBS) (GIBCO, Grand Island, NY, USA), 2 mM L-glutamine, 100 units/ml penicillin and streptomycin (GIBCO, Grand Island, NY, USA). Cells were incubated at 37 °C in a humidified atmosphere of 5% CO_2 maintenance. For the induction of primary cilia formation, cells were incubated in serum-starved media without FBS for 24–36 h.

2.3. Cell adaptation

Beas-2B cells were originally maintained in the coated dishes with FBS-free BEBE containing BEBM™ bronchial epithelial cell growth basal medium along with all the additives, BEGM™ kit (Lonza/Clonetics Co., Basel Switzerland). Due to that ACE2 was not detected in Beas-2B cells cultured with BEBE under our experimental condition (data not shown), cells were adapted by replacing BEBE to DMEM with 10% FBS in the following manner. Culture medium was sequentially exchanged by feeding the fresh BEBE containing 25%, 50%, 75% and 100% DMEM supplemented with 10% FBS every 24 h. After 5 days, cells were sub-cultured into uncoated dishes with DMEM containing 10% FBS. The cells were fully adapted by sub-culture up to 40 times after the start of adaptation. All experiments were performed with Beas-2B cells at 40th-60th passage.

2.4. Preparation of coated culture dish

Culture dishes were coated by the instruction on product sheet of Beas-2B cells (https://www.atcc.org/products/crl-9609#detailed-product-information) as follows. The coating solution was prepared by a mixture of 0.01 mg/ml fibronectin 0.03 mg/ml bovine collagen type I and 0.01 mg/ml BSA dissolved in BEBE. Culture dishes were treated with coating solution and agitated gently to coat the entire surface. Then, culture dishes were incubated in a 37 °C incubator overnight and coating solution was removed. Coated dishes were washed with PBS and stored at room temperature under light-protected condition up to one month.

2.5. Cytotoxicity assay

Cell survival was quantified by using colorimetric assay with MTT to measure intracellular succinate dehydrogenase content or by using luminescence assay with CellTiter-Glo substrate to measure intracellular ATP content [22]. For MTT assay, confluent cells were cultured with various concentrations of each reagent for 24 h. Cells were then incubated with 50 μg/ml of MTT at 37 °C for 2 h. Formazan formed by MTT were dissolved in dimethylsulfoxide (DMSO). Optical density (OD) was read at 540 nm. For CellTiter-Glo assay, cell cultures were treated with CellTiter-Glo substrate (Promega, Madison, WI, USA). Luminescence was detected by using Glomax® luminometer (Promega, Madison, WI, USA).

2.6. Transfection of nucleic acids

ACE2, receptor for SARS-Cov2 spike protein was overexpressed by the transfection of cells with pCMV3-ACE2-Flag plasmid DNA, which was accompanied with pCMV for control group, respectively. Each plasmid DNA was transfected into cells as follows [23]. Briefly, each nucleic acid and Polyethylenimine (PEI) (Polysciences, Inc., Warrington, PA, USA) was diluted in serum-free medium and incubated for 5 min, respectively. The diluted nucleic acid and PEI were mixed by inverting and incubated for 20 min to form complexes. Pre-formed complexes were added directly to the cells and cells were incubated for 24–48 h until use [23].

2.7. Immunofluorescence staining

The binding of a biotinylated SARS-CoV-2 spike protein to ACE2 was detected as follows. HEK293T cells with the indicated condition were grown on coverslip for 24 h. Cells were transfected with Flag-tagged pCMV-ACE2 plasmid DNA, which was accompanied with pCMV for control group (Mock) and incubated for 24 h. Cells were fixed with 4% paraformaldehyde (PFA) solution freshly prepared in phosphate buffered saline(PBS) for 10 min and permeabilized with 0.1% Triton X-100 in PBS. Then, cells were incubated with a biotinylated SARS-CoV-2 spike protein followed by the incubation with FITC-conjugated streptavidin for 20 min. Nucleus was visualized by staining cells with DAPI. Cells were observed and photographed at 1000 x magnification under a fluorescence microscope (Nikon, Tokyo, Japan).

2.8. Measurement of SARS-CoV-2 spike protein−ACE2 interactions

Inhibitory effect of UDCA on SARS-CoV-2 spike protein (SP)−ACE2

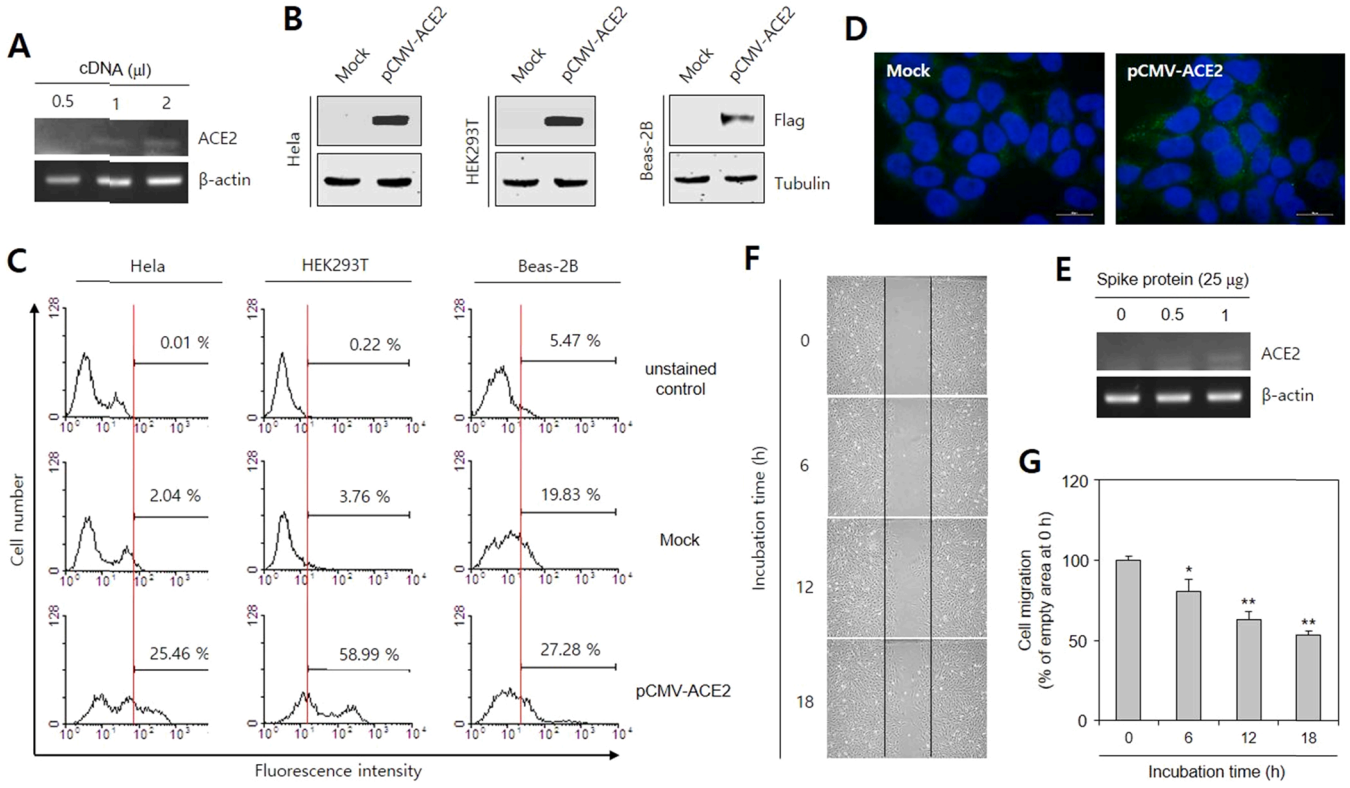

Fig. 1. Beas-2B cells bound SARS-CoV-2 spike protein and migrated time-dependently. (A) Total RNA was extracted from Beas-2B cells by using NucleoZol reagent and ACE2 transcripts were detected by PCR. (B-D) HeLa, HEK293T and Beas-2B cells were transfected with Flag-tagged pCMV-ACE2 plasmid DNA which was accompanied with pCMV for control group (Mock). Each cell was incubated with a biotinylated SARS-CoV-2 spike protein (SP) followed by the incubation with PE-conjugated streptavidin. Cells were analyzed by flow cytometry (B). Cell lysates were prepared and the expression of ACE2 was detected by western blot analysis using anti-Flag antibodies (C). Cells were fixed, permeabilized and incubated with a biotinylated SP followed by the incubation with FITC-conjugated streptavidin and DAPI. SP binding was observed under fluorescence microscope. The representative fluorescence image was shown. Processing (such as changing brightness and contrast is applied equally to controls across the entire image (D). (E) Beas-2B cells were treated with 25 ng SARS-CoV-2 spike protein for 0.5 or 1 h. Total RNA was extracted by using NucleoZol reagent and ACE2 transcripts were detected by PCR. (F, G) Beas-2B cells were plated on 35-mm^2 dishes and incubated for 24 h. A confluent monolayer of Beas-2B cells was then scratched with a sterile pipet tip. Then, cells were incubated for 18 h. Migration of cells into the space left by the scratch was photographed using a phase-contrast microscope at 200 × magnification (F). Percentage of cell migration was quantified by the decrease of empty area remained at each time point compared to empty area of the 0-h time point using NIH image analysis software (version 1.62; National Institutes of Health). Data in bar graphs represented as means ± SD. *$p < 0.05$; **$p < 0.01$, significantly different from the 0-h group (G).

interactions was measured by a previous method modified [24]. Briefly, 5 × 10^5 Beas-2B cells were suspended in 2% FCS containing Hank's balanced salt solution (HBSS) and incubated with UDCA at 37 °C CO_2 incubator for 1 h. Then, 25 ng of a biotinylated SARS-CoV-2 (2019-nCoV) SP were added and incubated for an additional 1 h on ice. After washing cells with HBSS containing 2% FBS twice, cells were incubated with PE-conjugated streptavidin for 30 min on ice. Cells were washed twice and suspended with HBSS containing 2% FBS. Then, 10,000 cells were evaluated by CELLQuest™ software in FACScalibur™ (Becton Dickinson, San Jose, CA). SP binding rates on ACE2 in Beas-2B cells were analyzed by using FlowJo™ software (ver. 10.8.0).

2.9. Wound healing assay

Cell migration was measured as described previously, with minor modifications [22]. Briefly, when Beas-2B cells reached confluence in a 35-mm culture dish (Corning, NY, USA), three wound lines in the form of a cross were made by scratching the cellular layer with a plastic pipette tip. Floating cells were then washed out, and fresh medium was added. Cells were then incubated at 37 °C in a humidified atmosphere of 5% CO_2 maintenance. Narrowing of the wound was then monitored using a phase-contrast microscope beginning 6 h after the scratch. The size of the wound at each time point was then quantified using NIH image analysis software (Image J, version 1.62), and compared with that in the initiation of cell migration.

2.10. Single cell path tracking

Beas-2B cell culture dishes were focused under live cell imaging light microscope. Cells were treated with UDCA in the absence or presence of SARS-CoV-2 spike protein (SP). Video image of live cells were automatically taken for 18 h. Cells were tracked every 30 min. Changes in single cell path were analyzed by tracking program, ImageJ plugin MTrackJ (Version 1.5.0) and represented with two-dimensional Rose diagram. Each cell path was overlayed on a polar grid with the normalization of start points to the origin. Movement trajectory was presented in coordinates for each cell [25].

2.11. Reverse transcription polymerase chain reaction (RT-PCR)

Total RNA was extracted by using NucleoZol reagent (MACHEREY-NAGEL GmbH & Co., Duren, Germany). Complementary DNA (cDNA) was synthesized from 1 μg of isolated total RNA, oligo-dT_{18}, and superscript reverse transcriptase (Bioneer, Daejeon, Rep. of Korea) in a final volume of 20 μl. For standard PCR, 1 μl of template cDNA was amplified with Taq DNA polymerase. PCR amplification was performed with 25 ~ 35 thermocycles for 30 s at 95 °C, 30 s at 55 °C, and 60 s at 72 °C using human (h) oligonucleotide primers specific for ACE2 (sense: 5′-

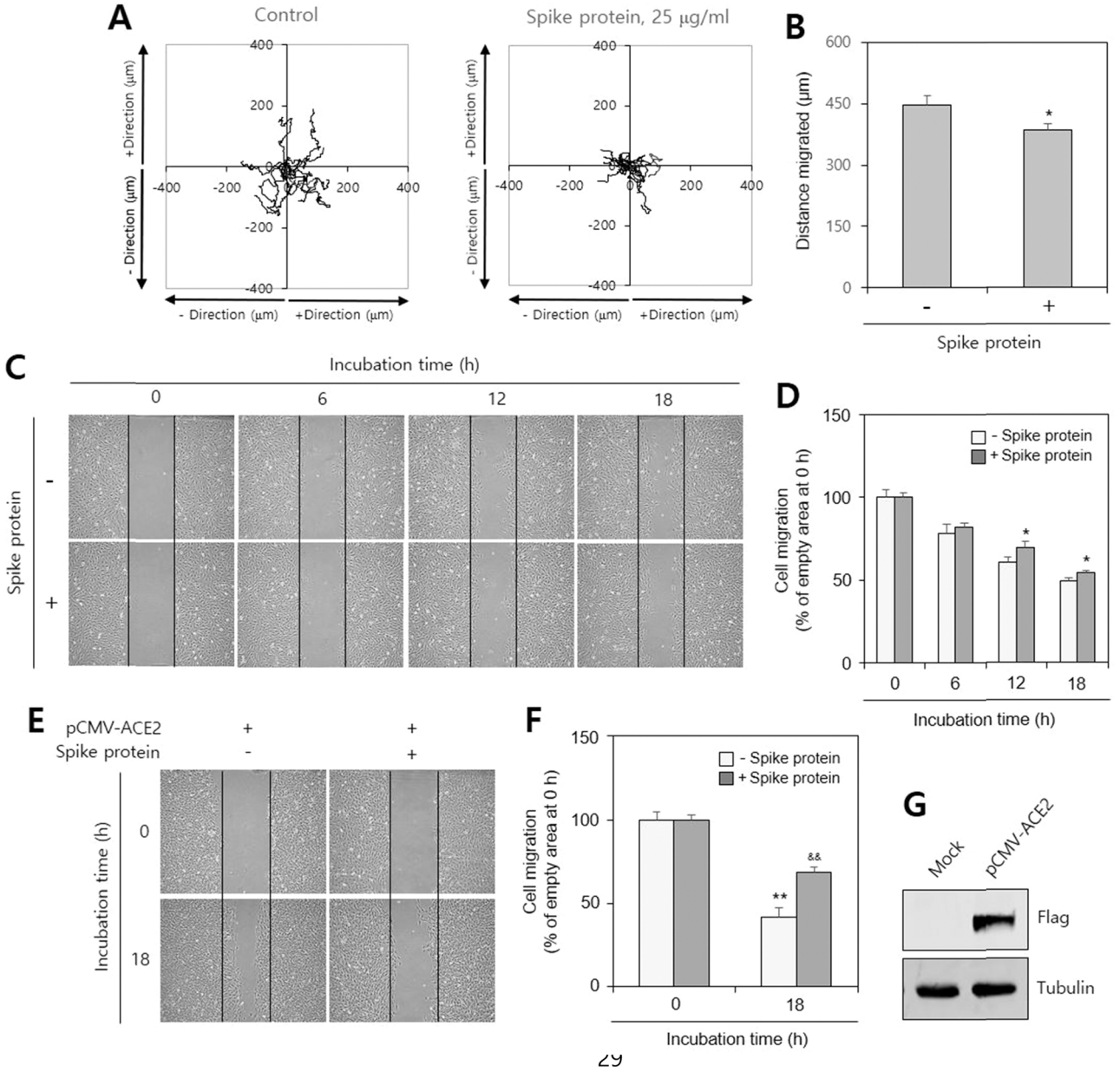

Fig. 2. Beas-2B cell migration was inhibited by the treatment with SARS-CoV-2 spike protein. (A, B) Beas-2B cells were treated with 25 ng/ml SARS-CoV-2 spike protein (SP). Changes in single cell path (A) and migrated distance of each cell (B) were analyzed by tracking program, ImageJ plugin MTrackJ (Version 1.5.0). Movement trajectory was presented in coordinates for each cell on a polar grid with the normalization of start points to the origin (A). Migrated distance was represented as a bar graph (B). (C-G) Beas-2B cells were plated on 35-mm^2 dishes and incubated for 24 h. Cells were transfected with Flag-tagged pCMV-ACE2 plasmid DNA which was accompanied with pCMV for control group (Mock) (E-G). A confluent monolayer of Beas-2B cells was then scratched with a sterile pipet tip. Then, cells were incubated with SP for 18 h. Migration of cells into the space left by the scratch was photographed using a phase-contrast microscope at 200 × magnification (C, E). Percentage of cell migration was quantified by the decrease of empty area remained at each time point compared to empty area of the 0-h time point using NIH image analysis software (version 1.62; National Institutes of Health) (D, F). Cell lysates were prepared and the expression of ACE2 was detected by western blot analysis using anti-Flag antibodies (G). Data in bar graphs represented as means ± SD. *$p < 0.05$; **$p < 0.01$, significantly different from SP-untreated control group at each time point (D, F).

cat tgg agc aag tgt tgg atc tt-3′; anti-sense: 5′-gag cta atg cat gcc att ctc a-3′) [26], and β-actin (sense: 5′-gtc acc aac tgg gac gac at-3; anti-sense: 5′-gca cag cct gga tag caa cg-3′). Amplified PCR products were separated by 1.0 ~ 1.5% agarose gel electrophoresis and detected on Ugenius 3® gel documentation system (Syngene, Cambridge, United Kingdom) [23].

2.12. Western blotting

Cells were lysed in ice-cold RIPA buffer (Triton X-100,) containing protease inhibitor (2 μg/ml aprotinin, 1μMpepstatin, 1 μg/ml leupeptin, 1 mM phenylmetylsufonyl fluoride (PMSF), 5 mM sodium fluoride (NaF) and 1 mM sodium orthovanadate (Na_3VO_4)). The protein concentration of the sample was measured using SMART™ BCA protein assay kit (Pierce 23228) from iNtRON Biotech. Inc. (Seoul, Rep. of Korea). Same amount of heat-denatured protein in sodium dodecyl sulfate (SDS) sample buffer was separated in sodium dodecyl sulfate polyacrylamide gel electrophoresis (SDS-PAGE), and then transferred to nitrocellulose membrane by using electro blotter. Equal amount of loaded sample on membrane was verified by ponceau S staining. The membrane was incubated with blocking solution (5% non-fat skim milk in Tris-buffered

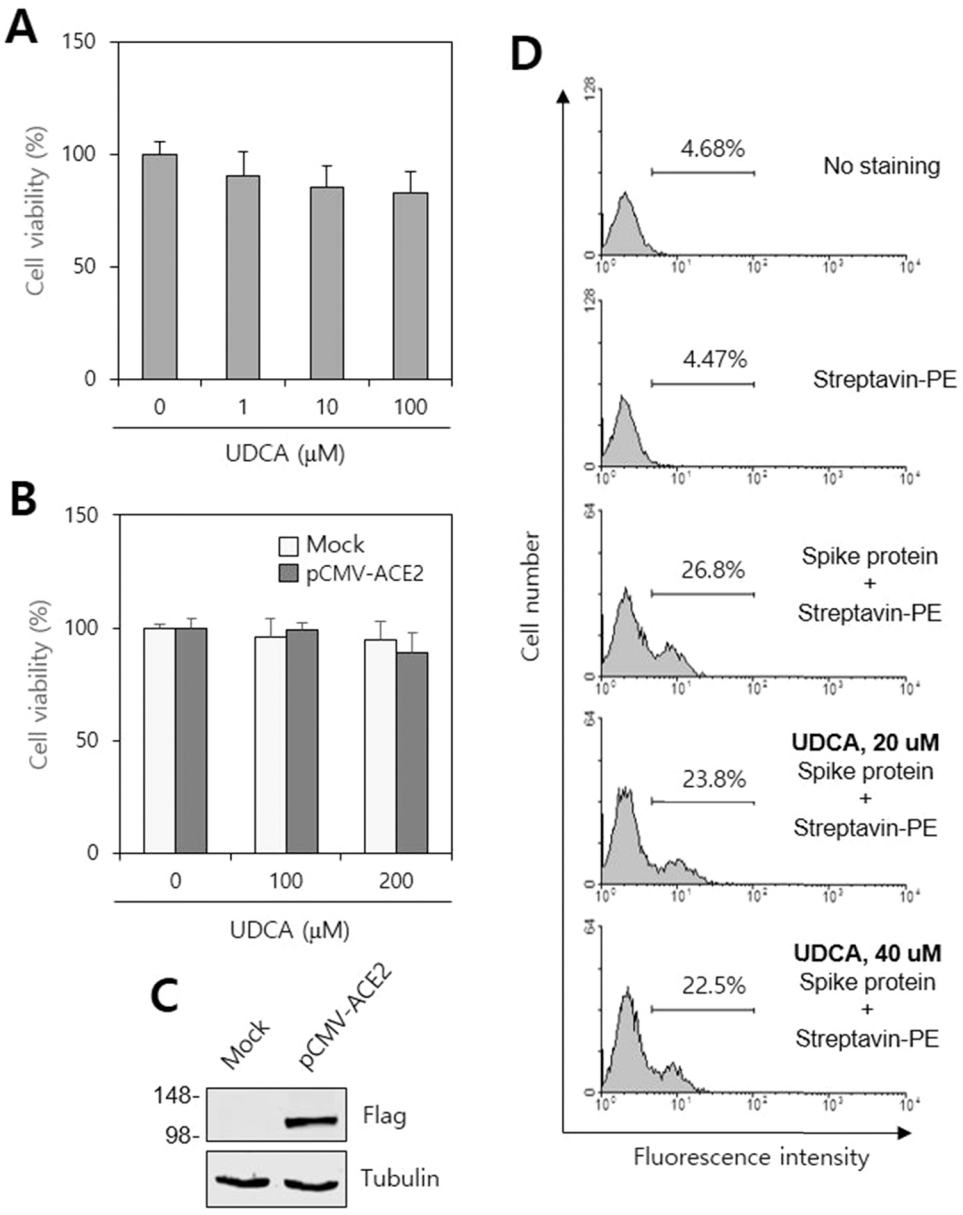

Fig. 3. Ursodeoxycholic acid inhibited SARS-CoV-2 spike protein-ACE2 interaction. (A) Beas-2B cells were treated with various concentrations of ursodeoxycholic acid (UDCA) for 24 h. Cell viability was measured by MTT assay. (B-D) Cells were transfected with Flag-tagged pCMV-ACE2 plasmid DNA which was accompanied with pCMV for control group (Mock) and incubated for 24 h . Then, cells were treated with 100 or 200 μM UDCA for 24 h. Cell viability was measured by CellTiter-Glo assay (B). Cell lysates were prepared and the expression of ACE2 was detected by western blot analysis using anti-Flag antibodies (C). Cells were pre-incubated with 20 or 40 μM UDCA at 37 °C CO_2 incubator for 1 h. Then, a biotinylated SARS-CoV-2 spike protein were added and incubated for an additional 1 h on ice. After washing cells with HBSS containing 2% FBS twice, cells were incubated with PE-conjugated streptavidin for 30 min on ice. Cells were washed with HBSS and analyzed by CELLQuest™ software in FACScalibur™ (D).

saline with Tween 20 (TBST)), and then followed by incubation with the specific primary antibodies. Horse radish peroxidase (HRP)- or infrared (IR) fluorescence dye -conjugated secondary antibody were used for target-specific primary antibody. Immuno-reactive target bands were visualized by the reaction with enhanced chemiluminescence (ECL-PS250) (Dongin LS, Seoul, Rep. of Korea) on X-ray film (Agfa HealthCare, Seol, Rep. of Korea) or by the detection of IRdye with Odyssey CLx Infrared Imaging System (LI-COR Biosciences, Lincoln, NE, Germany), respectively [23].

2.13. Statistical analysis

Experimental differences were verified for statistical significance using ANOVA and student's t- BEAS-2B cell migration was faster in the medium including FBS compared to that under serum starvation.test. P value of < 0.05 and < 0.01 was considered to be significant.

3. Results

3.1. SARS-CoV-2 SP bound to ACE2 on Beas-2B cells

SARS-CoV-2 employs the ACE2 SARS-CoV receptor for cellular entry [5,8]. Then, we examined the interaction of SARS-CoV-2 SP and ACE2 on Beas-2B human bronchial epithelial cells. The results showed that Beas-2B cells expressed ACE2 (Fig. 1A). SP–ACE2 interaction was confirmed through the overexpression of ACE2 into HeLa, HEK293T, and Beas-2B cells using flag-tagged pCMV-ACE2 plasmid DNA (Fig. 1B). The SP–ACE2 interaction in each cell line was also assessed by using flow cytometry analysis. SP binding rates on ACE2 in pCMV-transfected (mock) HeLa, HEK293T, and Beas-2B cells were 2.04%, 3.76%, and 19.83%, compared to 0.01%, 0.22%, and 5.47% in unstained control cells, respectively. SP binding rates on ACE2 in pCMV-ACE2-transfected HeLa, HEK293T, and Beas-2B cells were 25.46%, 58.99%, and 27.28% higher compared to those in pCMV-transfected cells, respectively (Fig. 1C). SP binding on pCMV-ACE2-transfected Beas-2B cells was also observed by immunofluorescence staining (Fig. 1D). ACE2 expression was increased by SP treatment (Fig. 1E). Because airway epithelial cell

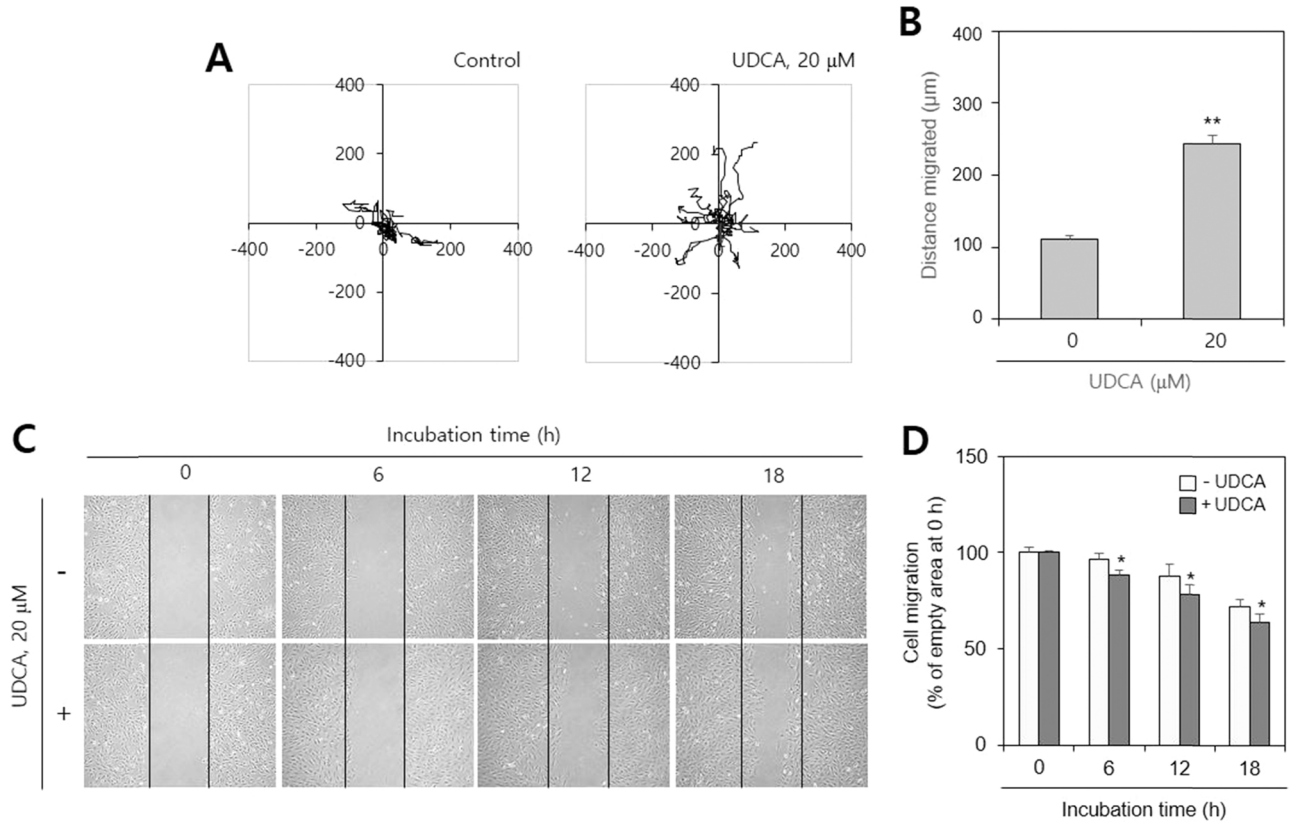

Fig. 4. Beas-2B cell migration was enhanced by the treatment with ursodeoxycholic acid. (A, B) Beas-2B cells were treated with 20 μM ursodeoxycholic acid (UDCA). Changes in single cell path (A) and migrated distance of each cell (B) were analyzed by tracking program, ImageJ plugin MTrackJ (Version 1.5.0). Movement trajectory was presented in coordinates for each cell on a polar grid with the normalization of start points to the origin (A). Migrated distance was represented as a bar graph (B). (C, D) Beas-2B cells were plated on 35-mm^2 dishes and incubated for 24 h. A confluent monolayer of Beas-2B cells was then scratched with a sterile pipet tip. Then, cells were incubated with UDCA for 18 h. Migration of cells into the space left by the scratch was photographed using a phase-contrast microscope at 200 × magnification (C). Percentage of cell migration was quantified by the decrease of empty area remained at each time point compared to empty area of the 0-h time point using NIH image analysis software (version 1.62; National Institutes of Health) (D). Data in bar graphs represented as means ± SD. *$p < 0.05$; ** $p < 0.01$, significantly different from UDCA-untreated control group (B) at each time point (D).

migration plays a pivotal role in airway repair [12], we tested whether Beas-2B cells could migrate after wounding. Beas-2B cell migration was faster in medium including fetal bovine serum (FBS) than under conditions of serum starvation (data not shown). When a monolayer of Beas-2B cells was scratched, we observed approximately 55% cell migration after 18 h of incubation (Fig. 1F, G). These findings suggest that Beas-2B cells are appropriate for testing changes in airway epithelia caused by SP.

3.2. SARS-CoV-2 SP inhibited Beas-2B cell migration

The effect of SP on airway epithelial cell migration was examined by the measurement of changes in Beas-2B cell migration using single cell path tracking. Following SP treatment, Beas-2B cell migration was significantly reduced (Fig. 2A) and the total cell migration distance was decreased (Fig. 2B). A monolayer of Beas-2B cells was scratched and treated with SP, and cell migration was reduced by approximately 15–10% after 12–18 h of incubation (Fig. 2C, D), confirming that airway cell migration was inhibited in pCMV-ACE2-transfected Beas-2B cells. Cell migration was more significantly inhibited (~40%) by SP treatment in ACE2-overexpressed cells following 18 h of incubation compared to control (Fig. 2E, F). ACE2 overexpression was detected by Western blot analysis (Fig. 2G). These results suggest that airway epithelia can be injured through SP–ACE2 interaction.

3.3. UDCA inhibited SARS-CoV-2 SP–ACE2 interaction

Membrane-bound UDCA may reduce the internalization of SARS-CoV-2 in the host cell [20]. Therefore, we investigated whether UDCA can prevent SP binding on ACE2. We detected no changes in the viability of Beas-2B cells (Fig. 3A) or ACE2-overexpressed cells (Fig. 3B) following UDCA treatment up to a concentration of 100 μM. According to flow cytometry analysis, overexpression of ACE2 in Beas-2B cells (Fig. 3C) pretreated with UDCA inhibited the SP–ACE2 interaction. SP-ACE2 interaction rates were 23.8% and 22.5% in the 20 and 40 μM UDCA pretreatment groups, respectively, compared to 26.5% in the control group (Fig. 3D), suggesting that UDCA may inhibit SP binding on ACE2.

3.4. UDCA ameliorated Beas-2B cell migration inhibited by SARS-CoV-2 SP

Furthermore, we investigated whether UDCA could recover SP-mediated inhibition of airway cell migration. Cells were incubated with 20 μM UDCA, and the increase in cell migration was measured by single cell path tracking (Fig. 4A). The total distance of cell migration increased 2.5-fold following UDCA treatment compared to the control (Fig. 4B). A wound healing assay showed that cell migration was enhanced approximately 10–15% following UDCA treatment compared to control (Fig. 4C, D). In cells treated with SP in the absence or presence of UDCA, SP-mediated single cell path tracking was ameliorated by UDCA treatment compared to the UDCA-untreated control (Fig. 5A).

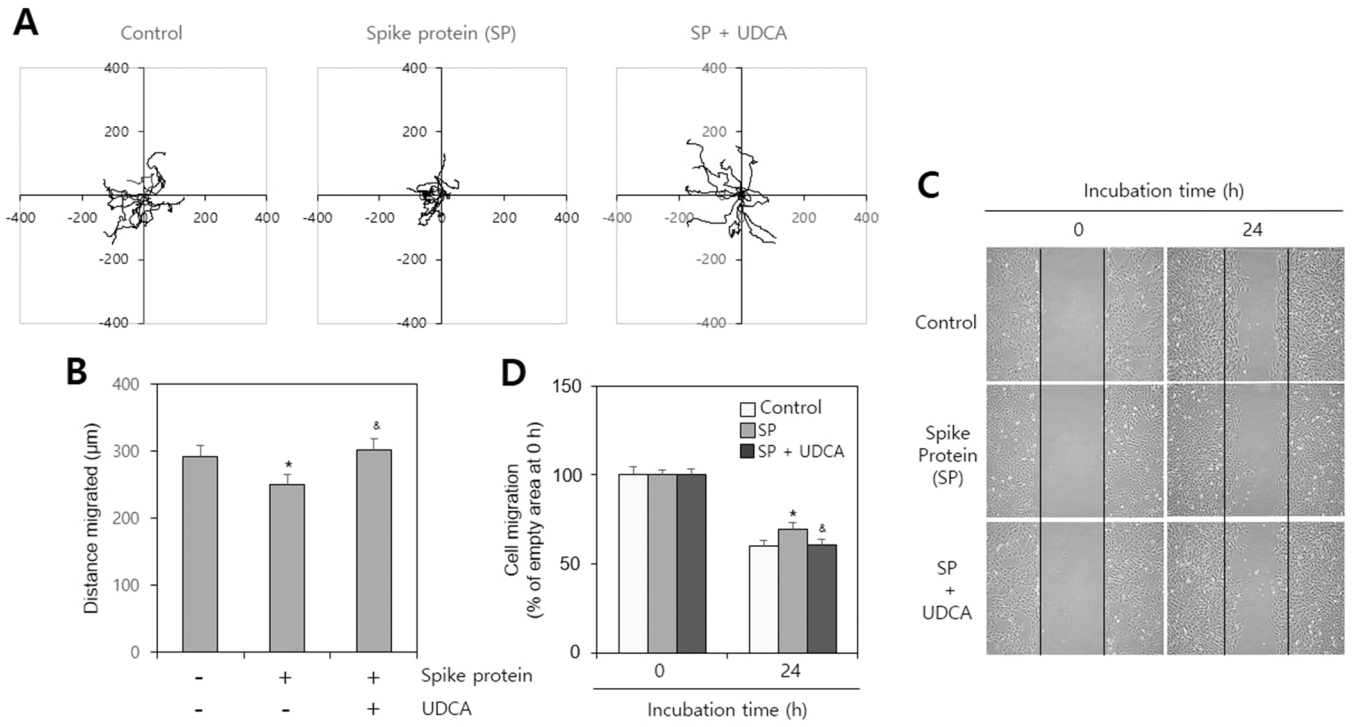

Fig. 5. Ursodeoxycholic acid attenuated inhibitory effect of SARS-CoV-2 spike protein on Beas-2B cell migration. (A, B) Beas-2B cells were treated with SARS-CoV-2 spike protein (SP) in the absence or presence of 20 μM ursodeoxycholic acid (UDCA). Changes in single cell path (A) and migrated distance of each cell (B) were analyzed by tracking program, ImageJ plugin MTrackJ (Version 1.5.0). Movement trajectory was presented in coordinates for each cell on a polar grid with the normalization of start points to the origin (A). Migrated distance was represented as a bar graph (B). (C, D) Beas-2B cells were plated on 35-mm^2 dishes and incubated for 24 h. A confluent monolayer of Beas-2B cells was then scratched with a sterile pipet tip. Then, cells were incubated with SP in the absence or presence of 20 μM UDCA for 24 h. Migration of cells into the space left by the scratch was photographed using a phase-contrast microscope at 200 × magnification (C). Percentage of cell migration was quantified by the decrease of empty area remained at each time point compared to empty area of the 0-h time point using NIH image analysis software (version 1.62; National Institutes of Health) (D). Data in bar graphs represented as means ± SD. $^*p < 0.05$, significantly different from SP-untreated control group. $^{\&}p < 0.05$, significantly different from SP-treated group (B, D).

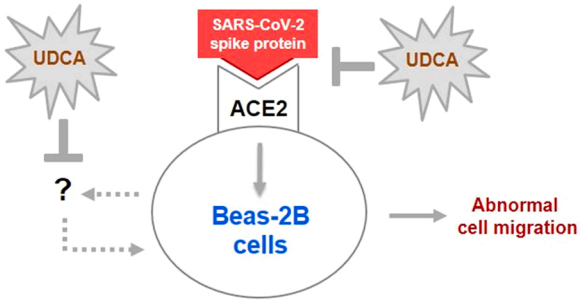

Fig. 6. Scheme about action of UDCA on Beas-2B cell migration. Beas-2B cell migration might be retarded by binding SARS-CoV-2 spike protein (SP) to ACE2 receptor followed by the production of some molecules and their action which were represented as '?' and gray dotted lines, respectively. UDCA could be effective to restore SP-mediated inhibition of Beas-2B cell migration by the interference of SP-ACE2 interaction or the inhibition of some molecules. Our findings are presented by gray solid lines.

The total distance of cell migration was increased by approximately 20% in cells co-incubated with UDCA and SP compared to the control group (Fig. 5B). The recovery of SP-mediated cell migration was confirmed by a wound healing assay (Fig. 5C). Cell migration by SP treatment was enhanced approximately 15% following incubation with UDCA for 24 h compared to the control (Fig. 5D). Together, these data suggest that UDCA may be a novel molecule for the prevention of SARS-CoV-2 binding on ACE2 and abnormal airway cell migration (Fig. 6).

4. Discussion

COVID-19 is caused by SARS-CoV-2 [1]. Airway epithelial cells play a role in protecting the airway mucosa from various types of injury [9–11]. In particular, airway epithelial cell migration plays a pivotal role in airway repair [12,13]. Therefore, it is important to determine whether SARS-CoV-2 impairs airway epithelial cell migration, which can be attenuated by various molecules. UDCA interacts in two distinct regions of SP sequences, and may also bind to the cell membrane to inhibit SARS-CoV-2 entry into host cells [20]. However, the physiological effects of UDCA on airway epithelium regeneration remain poorly understood. In this study, we investigated whether UDCA could help the restoration of bronchial epithelial layer using BEAS-2B cells. Our data demonstrate that UDCA can contribute to the inhibition of abnormal airway epithelial cell migration.

The SARS-CoV-2 SP uses ACE2 for entry [5] after an RBD of the SP recognizes ACE2 as a receptor on the membrane [7]. The interaction of SARS-CoV-2 SP and ACE2 is a major determinant of virus replication and disease severity [5,8]. Our data showed that SP binds to control and ACE2-overexpressed Beas-2B cells (Fig. 1). SP treatment delayed the migration of both control and ACE2-overexpressed Beas-2B cells (Fig. 2), and UDCA interfered with the binding of SP to ACE2 (Fig. 3). These findings suggest that UDCA can enhance both the repair mechanism, to prevent damage caused by SP–ACE2 interaction, and restoration of the epithelial basal layer.

Previous studies have demonstrated that various molecules are associated with signaling pathways involved in cell migration. Although many studies have reported a correlation between cell migration and the repair of damaged airway epithelium, the mechanism by which UDCA

influences the regenerative migration of airway epithelial cells has remained controversial. Rapid re-epithelialization is promoted by microcirculation-derived factors, together with an intact basement membrane [13]. Actin polymerization is involved in airway epithelial cell migration and repair [27,28]. Cell migration involves anchorage onto type IV collagen via focal contacts, and metalloproteinases control repair cell migration by remodeling the provisional extracellular matrix [29]. In this study, Beas-2B cell migration was increased by UDCA treatment (Fig. 4) Therefore, further study of the mechanism underlying the effects of UDCA on cell migration is required.

The role of UDCA-mediated cell migration in epithelium regeneration following damage was examined by the effect of SP on airway epithelial cell migration. A wound healing assay and single cell path tracking showed that SP decreased airway epithelial cell migration, which was recovered by UDCA treatment (Fig. 5). This finding suggests that UDCA can regenerate SP-mediated abnormal migration of airway epithelial cells.

Although our results do not provide a straightforward explanation of the mechanism of UDCA action in SP-mediated cell migration, we demonstrated that UDCA can recover abnormal epithelial cell migration following airway damage. However, the signaling molecules that regulate cell migration and their mechanism remain unclear, and many questions remain about the mechanisms of SP- and UDCA-mediated cell migration. It is also required to further validate our data through in vivo studies.

Anti-inflammatory function of UDCA in bronchial epithelium may be a possible mechanism as previously proposed in the literature with in vivo lung injury model [17, 30, 31]. Pre-treatment with UDCA remarkably alleviated the pathologic and biochemical changes by in vivo perinephric fat which induced acute lung injury and respiratory distress syndrome in rats [30]. UDCA attenuated pulmonary edema and lung inflammation induced by lipopolysaccharide in rats [31]. UDCA also suppress mouse eosinophilic airway inflammation by inhibiting the function of dendritic cells (DC) through the expression of nuclear farnesoid X receptor and by modulating the DC/T cell interaction [17]. So, these reports could indirectly support our results that UDCA-induced cell migration prevent damage caused by SP–ACE2 interaction and enhance restoration of the epithelial basal layer.

Our results are summarized in Fig. 6, which shows the amelioration of SP-mediated airway epithelial cell migration due to interference by the SP–ACE2 interaction or the inhibition of signaling molecules. Together, our findings suggest that UDCA could represent a therapeutic molecule for restoring airway epithelial cell damage caused by SARS-CoV-2, and that UDCA may be useful in treating certain types of structural changes in individual airways exposed to various types of injury.

CRediT authorship contribution statement

PXT settled down and conducted the experiments, and wrote primary manuscript. **TDDB** conducted the experiments and analyzed the results. **EYM** planed main idea of the study, analyzed the results, corrected the manuscript, and supported **PXT** and **TDDB** to provide reagents, materials and analysis tools. All authors reviewed the manuscript. Authors certify that all authors have seen and approved the final version of the manuscript being submitted. They warrant that the article is the authors' original work, has not received prior publication and is not under consideration for publication elsewhere.

Conflict of interest statement

The authors declare no competing financial and non- financial interests.

Data availability

The authors do not have permission to share data.

Acknowledgement

We sincerely thank Tae-Kyu Jang and Seo-Yeon Choi for their technical assistance to experiments of wound healing assay and single cell path tracking. This research was supported by the Basic Research Program through the National Research Foundation of Korea (NRF) funded by the Ministry of Science and ICT (grant number 2021R1A4A5033289).

References

[1] T.C. Masters-Waage, N. Jha, J. Reb, COVID-19, Coronavirus, wuhan virus, or China virus? Understanding how to "Do No Harm" when naming an infectious disease, Front. Psychol. 11 (2020), 561270.
[2] N. Chen, M. Zhou, X. Dong, J. Qu, F. Gong, Y. Han, Y. Qiu, J. Wang, Y. Liu, Y. Wei, J. Xia, T. Yu, X. Zhang, L. Zhang, Epidemiological and clinical characteristics of 99 cases of 2019 novel coronavirus pneumonia in Wuhan, China: a descriptive study, Lancet 395 (10223) (2020) 507–513.
[3] F. Wu, S. Zhao, B. Yu, Y.M. Chen, W. Wang, Z.G. Song, Y. Hu, Z.W. Tao, J.H. Tian, Y.Y. Pei, M.L. Yuan, Y.L. Zhang, F.H. Dai, Y. Liu, Q.M. Wang, J.J. Zheng, L. Xu, E. C. Holmes, Y.Z. Zhang, A new coronavirus associated with human respiratory disease in China, Nature 579 (7798) (2020) 265–269.
[4] N. Zhu, D. Zhang, W. Wang, X. Li, B. Yang, J. Song, X. Zhao, B. Huang, W. Shi, R. Lu, P. Niu, F. Zhan, X. Ma, D. Wang, W. Xu, G. Wu, G.F. Gao, W. Tan, I. China Novel Coronavirus, T. Research, A. Novel, Coronavirus from Patients with Pneumonia in China, 2019, N. Engl. J. Med. 382 (8) (2020) 727–733.
[5] M. Hoffmann, H. Kleine-Weber, S. Schroeder, N. Kruger, T. Herrler, S. Erichsen, T. S. Schiergens, G. Herrler, N.H. Wu, A. Nitsche, M.A. Muller, C. Drosten, S. Pohlmann, SARS-CoV-2 cell entry depends on ACE2 and TMPRSS2 and is blocked by a clinically proven protease inhibitor, Cell 181 (2) (2020) 271–280 e8.
[6] F. Li, M. Berardi, W. Li, M. Farzan, P.R. Dormitzer, S.C. Harrison, Conformational states of the severe acute respiratory syndrome coronavirus spike protein ectodomain, J. Virol. 80 (14) (2006) 6794–6800.
[7] X. Xiao, D.S. Dimitrov, The SARS-CoV S glycoprotein, Cell Mol. Life Sci. 61 (19–20) (2004) 2428–2430.
[8] P. Zhou, X.L. Yang, X.G. Wang, B. Hu, L. Zhang, W. Zhang, H.R. Si, Y. Zhu, B. Li, C. L. Huang, H.D. Chen, J. Chen, Y. Luo, H. Guo, R.D. Jiang, M.Q. Liu, Y. Chen, X. R. Shen, X. Wang, X.S. Zheng, K. Zhao, Q.J. Chen, F. Deng, L.L. Liu, B. Yan, F. X. Zhan, Y.Y. Wang, G.F. Xiao, Z.L. Shi, A pneumonia outbreak associated with a new coronavirus of probable bat origin, Nature 579 (7798) (2020) 270–273.
[9] E. Puchelle, J.M. Zahm, J.M. Tournier, C. Coraux, Airway epithelial repair, regeneration, and remodeling after injury in chronic obstructive pulmonary disease, Proc. Am. Thorac. Soc. 3 (8) (2006) 726–733.
[10] S.T. Holgate, The airway epithelium is central to the pathogenesis of asthma, Allergol. Int. 57 (1) (2008) 1–10.
[11] T.R. Martin, C.W. Frevert, Innate immunity in the lungs, Proc. Am. Thorac. Soc. 2 (5) (2005), 403-11.
[12] W.C. Wang, C.Y. Kuo, B.S. Tzang, H.M. Chen, S.H. Kao, IL-6 augmented motility of airway epithelial cell BEAS-2B via Akt/GSK-3beta signaling pathway, J. Cell Biochem. 113 (11) (2012), 3567-75.
[13] M. Oertel, A. Graness, L. Thim, F. Buhling, H. Kalbacher, W. Hoffmann, Trefoil factor family-peptides promote migration of human bronchial epithelial cells: synergistic effect with epidermal growth factor, Am. J. Respir. Cell Mol. Biol. 25 (4) (2001), 418-24.
[14] G. Paumgartner, U. Beuers, Ursodeoxycholic acid in cholestatic liver disease: mechanisms of action and therapeutic use revisited, Hepatology 36 (3) (2002) 525–531.
[15] M.S. Mroz, B.J. Harvey, Ursodeoxycholic acid inhibits ENaC and Na/K pump activity to restore airway surface liquid height in cystic fibrosis bronchial epithelial cells, Steroids 151 (2019), 108461.
[16] S. Miyaguchi, M. Mori, Ursodeoxycholic acid (UDCA) suppresses liver interleukin2 mRNA in the cholangitis model, Hepatogastroenterology 52 (62) (2005) 596–602.
[17] M.A. Willart, M. van Nimwegen, A. Grefhorst, H. Hammad, L. Moons, H. C. Hoogsteden, B.N. Lambrecht, A. Kleinjan, Ursodeoxycholic acid suppresses eosinophilic airway inflammation by inhibiting the function of dendritic cells through the nuclear farnesoid X receptor, Allergy 67 (12) (2012) 1501–1510.
[18] E.K. Kim, J.H. Cho, E. Kim, Y.J. Kim, Ursodeoxycholic acid inhibits the proliferation of colon cancer cells by regulating oxidative stress and cancer stem-like cell growth, PLoS One 12 (7) (2017), e0181183.
[19] N.F. Abdelkader, M.M. Safar, H.A. Salem, Ursodeoxycholic acid ameliorates apoptotic cascade in the Rotenone model of Parkinson's disease: modulation of mitochondrial perturbations, Mol. Neurobiol. 53 (2) (2016) 810–817.
[20] F.J. Rodal Canales, L. Perez-Campos Mayoral, M.T. Hernandez-Huerta, L. M. Sanchez Navarro, C.A. Matias-Cervantes, M. Martinez Cruz, E. Cruz Parada, E. Zenteno, E.G. Ramos-Martinez, E. Perez-Campos Mayoral, C. Romero Diaz, E. Perez-Campos, Interaction of Spike protein and lipid membrane of SARS-CoV-2 with Ursodeoxycholic acid, an in-silico analysis, Sci. Rep. 11 (1) (2021) 22288.
[21] A. Carino, F. Moraca, B. Fiorillo, S. Marchiano, V. Sepe, M. Biagioli, C. Finamore, S. Bozza, D. Francisci, E. Distrutti, B. Catalanotti, A. Zampella, S. Fiorucci, Hijacking SARS-CoV-2/ACE2 receptor interaction by natural and semi-synthetic steroidal agents acting on functional pockets on the receptor binding domain, Front. Chem. 8 (2020), 572885.

[22] J.W. Jang, J.W. Lee, Y.D. Yoon, J.S. Kang, E.Y. Moon, Bisphenol A and its substitutes regulate human B cell survival via Nrf2 expression, Environ. Pollut. 259 (2020), 113907.
[23] J.W. Lee, H.S. Kim, E.Y. Moon, Thymosin beta-4 is a novel regulator for primary cilium formation by nephronophthisis 3 in HeLa human cervical cancer cells, Sci. Rep. 9 (1) (2019) 6849.
[24] J. Moreaux, E. Legouffe, E. Jourdan, P. Quittet, T. Reme, C. Lugagne, P. Moine, J. F. Rossi, B. Klein, K. Tarte, BAFF and APRIL protect myeloma cells from apoptosis induced by interleukin 6 deprivation and dexamethasone, Blood 103 (8) (2004) 3148–3157.
[25] B. Gweon, T.K. Jang, P.X. Thuy, E.Y. Moon, Primary Cilium by Polyinosinic: Polycytidylic Acid Regulates the Regenerative Migration of Beas-2B Bronchial Epithelial Cells, Biomol Ther (Seoul) 30 (2) (2022) 170–178.
[26] L. Tao, Y. Qiu, X. Fu, R. Lin, C. Lei, J. Wang, B. Lei, Angiotensin-converting enzyme 2 activator diminazene aceturate prevents lipopolysaccharide-induced inflammation by inhibiting MAPK and NF-kappaB pathways in human retinal pigment epithelium, J. Neuroinflamm. 13 (2016) 35.
[27] S. de Bentzmann, M. Polette, J.M. Zahm, J. Hinnrasky, C. Kileztky, O. Bajolet, J. M. Klossek, A. Filloux, A. Lazdunski, E. Puchelle, Pseudomonas aeruginosa virulence factors delay airway epithelial wound repair by altering the actin cytoskeleton and inducing overactivation of epithelial matrix metalloproteinase-2, Lab. Investig. 80 (2) (2000) 209–219.
[28] J.M. Zahm, M. Chevillard, E. Puchelle, Wound repair of human surface respiratory epithelium, Am. J. Respir. Cell Mol. Biol. 5 (3) (1991) 242–248.
[29] N. Castillon, J. Hinnrasky, J.M. Zahm, H. Kaplan, N. Bonnet, P. Corlieu, J. M. Klossek, K. Taouil, A. Avril-Delplanque, B. Peault, E. Puchelle, Polarized expression of cystic fibrosis transmembrane conductance regulator and associated epithelial proteins during the regeneration of human airway surface epithelium in three-dimensional culture, Lab. Investig. 82 (8) (2002) 989–998.
[30] F. Niu, H. Li, X. Xu, L. Sun, N. Gan, A. Wang, Ursodeoxycholic acid protects against lung injury induced by fat embolism syndrome, J. Cell. Mol. Med. 24 (24) (2020) 14626–14632.
[31] F. Niu, X. Xu, R. Zhang, L. Sun, N. Gan, A. Wang, Ursodeoxycholic acid stimulates alveolar fluid clearance in LPS-induced pulmonary edema via ALX/cAMP/PI3K pathway, J. Cell Physiol. 234 (11) (2019) 20057–20065.